Non-Isolated Reduced Redundant Power Processing DC/DC Converters: A Systematic Study of Topologies With Wide Voltage Ratio for High-Power Applications

Charoula G. Zogogianni, Emmanuel C. Tatakis, and Marko S. Vekic

***Abstract*—In this paper, a systematic and analytical study of non-isolated topologies belonging to the family of reduced redundant power processing (R2P2) converters is presented. Based on this study, all the non-isolated R2P2 topologies that can be implemented in reality are derived. Detailed examples clarify all possible cases of this analysis. In addition to this, the voltage ratio and the efficiency for each one of the R2P2 configurations are calculated, being further illustrated with examples. A comparison among configurations is also discussed with criteria the high step-up voltage gain and efficiency, aiming for high-power applications. One of these R2P2 converters is selected for further examination, as the most suitable for such applications. The theoretical analysis, as well as the calculations of the step-up voltage ratio and efficiency of the selected converter, is compared to experimental results conducted on a 2-kW laboratory prototype designed to operate in various step-up voltage ratios and in a high-power range, proving the effectiveness of the proposed investigation.**

***Index Terms*—DC–DC power conversion, high-power applications, high step-up voltage ratio, reduced redundant power processing (R2P2) converters, switched mode power supplies.**

I. Introduction

NOWADAYS, a variety of applications necessitates the employment of dc/dc converters, e.g., renewable energy systems, industrial applications, automotive industry, electric vehicles, etc. [1]–[4]. More specifically, systems that exploit renewable sources (photovoltaics, wind generators etc.), as well as fuel cells and thermoelectric generators (TEGs), require dc/dc

Manuscript received July 28, 2018; revised October 13, 2018; accepted December 7, 2018. Date of publication December 24, 2018; date of current version June 10, 2019. This work was supported by the State Scholarships Foundation (IKY) funded by the Action "Scholarship Program for postgraduate studies of second cycle" within the OP "Human Resources Development, Education and Lifelong Learning", 2014–2020, co-funded by the European Social Fund and Greek State. Recommended for publication by Associate Editor D. G. Lamar. *(Corresponding author: Charoula G. Zogogianni.)*

C. G. Zogogianni and E. C. Tatakis are with the Laboratory of Electromechanical Energy Conversion, Department of Electrical and Computer Engineering, University of Patras, Rion-Patras 26504, Greece (e-mail:

gain, while special attention was given to some topologies that can be transformed to single-switch equivalent counterparts. Nevertheless, their experimental prototypes are up to 100 W and step-up voltage ratio is up to 7. Furthermore, it is proven in [27] that the R2P2 topologies which can be transformed to single switch are not necessarily more efficient, since the conduction losses on the switch are dramatically increased, resulting in efficiency degradation. In [28], the R2P2 principle and the appropriate power flow graphs are applied for the derivation of double-input single-output converters; hence, their three-port network comprises two input sources and load instead of input port, energy storage element, and output port that is employed for SISO converters. This modified network produces different possible configurations compared to SISO ones, dedicated for applications with two different types of renewable energy sources. Their systematic study is out of the scope of the work presented in this paper.

Despite the efforts for classification of R2P2 configurations, there is not any derivation of all the implementable non-isolated combinations of basic converters (Bk, Bt and BB) within each R2P2 configuration. In addition to this, a systematic and analytical study for their voltage gain and efficiency in terms of their individual converters' characteristics has not still been presented in the literature. Moreover, most of the experiments are conducted within the range of 100–300 W, meaning that none of these converters has been tested in a high-power range, so that their functionality, efficiency, and step-up capability to be evaluated and compared with their estimated theoretical values. All of the aforementioned are the aim of this work.

In this paper, a general analysis of R2P2 non-isolated dc–dc converters is presented. The possible connection and topology cases are defined and all the implementable topologies are identified and listed, based on a procedure that helps to discard the non-realizable ones. Furthermore, a classification of the R2P2 non-isolated converters is conducted according to their voltage ratio and overall efficiency. Moreover, the selection of the most suitable R2P2 non-isolated converter for high voltage gain high-power applications, as well as specifications and some design guidelines for this converter, is also presented.

This paper is organized as follows. In Section II, the R2P2 concept is presented with more details and different connection cases are analyzed. Subsequently, the general rules for the selection of realizable R2P2 topologies are introduced and different topology cases that should be examined during selection are defined and analyzed. In Section III, examples are given for further clarification of the various cases and of the procedure for identifying the realizable topologies. Moreover, some conclusions are discussed for the selection procedure and all the realizable R2P2 non-isolated topologies are listed. In Section IV, the overall voltage ratio and the efficiency for each one of the non-isolated R2P2 configurations are calculated and clarified through analytical examples. In Section V, a brief comparison of the non-isolated R2P2 configurations is discussed for the selection of one topology among all, aiming to a high step-up high-power application, such as a waste heat recovery system (WHRS) for marine applications. Specifications and some design guidelines for the chosen topology are discussed in Section VI and experimental results are conducted for various step-up voltage ratios and in a high-power range, employing a prototype designed to handle power up to 2 kW. For improved efficiency, silicon carbide (SiC) semiconductor devices are also employed. Finally, conclusions are discussed in Section VII.

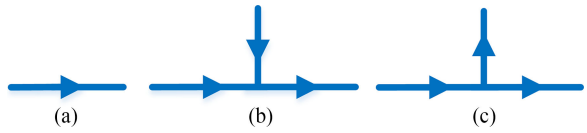

Fig. 1. Three possible types of power flow among ports of SISO R2P2 configurations [13]. (a) Type I. (b) Type II. (c) Type III.

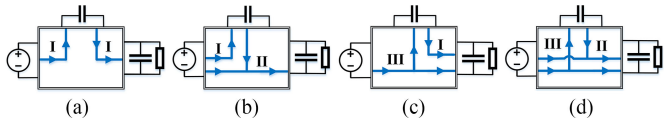

Fig. 2. Power flow graphs for constructing the SISO R2P2 configurations [13], [15]. (a) Type I-I. (b) Type I-II. (c) Type I-III. (d) Type II-III.

II. Definition of Connection Cases and Topology Cases for Non-Isolated R2P2 Converters

A. R2P2 Concept

The R2P2 concept employs a three-port network, namely input port, output port, and energy storage element, e.g., capacitor, and two converters A and B, placed in different power flow paths [13]. Since SISO topologies are considered for this paper, their input and output ports are unidirectional and positive, while the energy storage element can be bidirectional. Hence, three types of subgraphs, shown in Fig. 1, can be formed, indicating how one port can be connected to another in terms of power flow. Each subgraph is realized through power conversion, so a converter must be employed in order to connect one port with another. More specifically

1) Type I: The power is transferred from one port to another.
2) Type II: The power is transferred from two ports to one.
3) Type III: The power is transferred from one port to two.

Combining the above-described subgraphs of power flow among the ports of an R2P2 converter, four main types of power flow graphs, namely I-I, I-II, I-III, and II-III, are formed, as shown in Fig. 2.

Since each type includes two subgraphs, two converters, namely A and B, should be employed to realize each subgraph, resulting in 16 different R2P2 configurations [13]–[15], as illustrated in Fig. 3. The terms A, B, and C in the configuration names simply denote different realization of the same type, e.g., the type I-II can be realized in three different ways, named I-IIA, I-IIB, and I-IIC, resulting in three configurations. Also, the quantities k and m, shown in Fig. 3, designate per unit portions of the power split in the created nodes of the power flow graphs. Their calculation is dependent on the configuration and it is discussed in Section IV.

To transform the power flow graphs of the R2P2 concept into useful equivalent circuits, the basic connection rules described

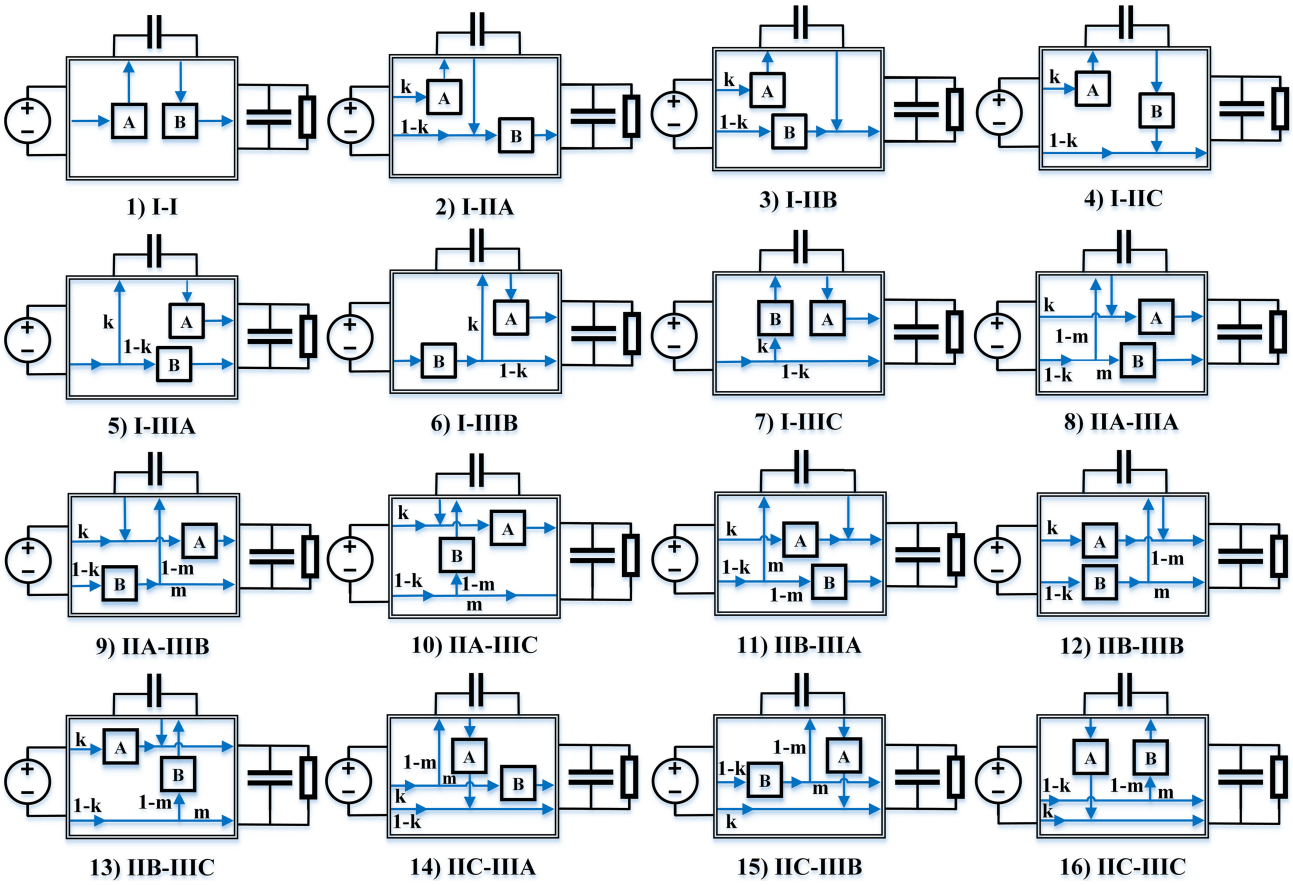

Fig. 3. Power flow graphs of the 16 configurations of R2P2 family of converters. A and B denote basic topologies and arrows indicate the power flow [13], [15].

in [15] must be followed, which are reproduced here for convenience.

1) Since the ports are voltage terminated, connection of any two ports simultaneously to a converter should be realized by a series connection of the ports' voltages.
2) Connection of a port with the inputs (or outputs) of two converters should be realized by a parallel circuit connection of the ports' voltages.

It is noted here that the series connection of two ports can be realized by their sum or subtraction, depending on the direction of power flow in the graphs. Furthermore, the series connection of two ports can be implemented in two ways, by alternating their position. Hence, in this paper, we add one more rule to the aforementioned.

3) For the series connection of two ports, either their sum or subtraction, two cases of electrical connections are possible (see Fig. 4).

Examples of the aforementioned cases of electrical connections for two different configurations are presented in Section III.

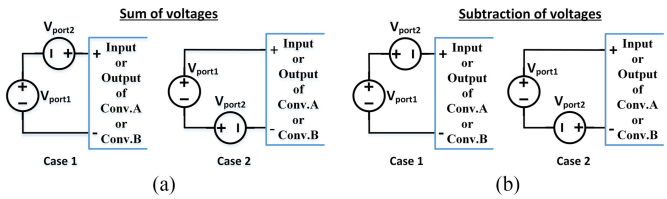

Fig. 4. Possible cases of electrical connections when two ports of the R2P2 concept are (a) added or (b) subtracted.

B. Identification of All Implementable Topologies

Each configuration imposes different electrical connections among ports and A, B converters (through its power flow graph and the three aforementioned rules). Taking this fact into account, as well as considering the type of employed A and B converters, it is possible to end up in realizable or non-realizable topologies.

Therefore, each combination should be examined first in terms of electrical connections and functionality in order to classify it as implementable topology or not. To this aim, a topology can be classified as non-implementable (and so it is rejected), if one or more of the following facts are met.

1) Short circuit (SC) in input/output of either the R2P2 configuration or the individual converters A and B.
2) SC in the capacitor of the R2P2 configuration.
3) Fixed output voltage of either the R2P2 configuration or the individual converters A and B, namely $M_A = 1$ or $M_B = 1$, leading to loss of controllability. The symbols M_A and M_B denote the voltage ratios of *A* and *B* converters, respectively.

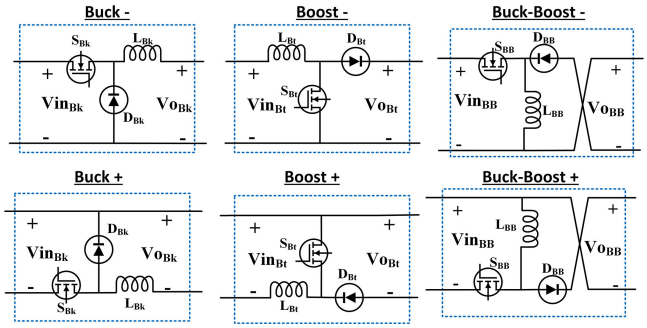

Fig. 5. Non-Isolated basic converters employed as A and B converters inside R2P2 configurations.

4) Negative voltage in input/output of either the R2P2 configuration or the individual converters A and B, since this is contradictory to the assumed positive polarity of the input/output of the basic converters.

C. Definition of Possible Cases and Combinations to be Examined

The converters A and B can be any topology. In this paper, the non-isolated basic converters Bk, Bt, and BB are employed in place of A and B converters for the study of non-isolated R2P2 combinations. For each of the basic converters, two cases of topologies are considered, as shown in Fig. 5. When the negative potential of their input is directly connected to one of the output potentials (negative for Bk and Bt and positive for BB), then we add the symbol—and we call these converters to belong to the negative polarity group of basic converters (Bk-, Bt-, BB-). Vice versa, when the positive potential of their input is directly connected to one of the output potentials (positive for Bk and Bt and negative for BB), then we add the symbol + and we call these converters to belong to the positive polarity group of basic converters (Bk+, Bt+, BB+).

In the power flow graphs (see Fig. 3), the R2P2 configuration of I-I type does not include any node where two ports are simultaneously connected, so there is only one case of electrical connections to be examined for realizable topologies. The R2P2 configurations of I-II and I-III types (three configurations of each type, see Section II-A) include one node where two ports are simultaneously connected. Hence, according to Rules 1 and 3, there are two possible cases of electrical connections to be examined for these configurations and so 12 equivalent circuits are created cumulatively. The R2P2 configurations of II-III type (nine in total) include two nodes, where two ports are simultaneously connected. Therefore, each node leads in two cases of electrical connections (according to Rule 3), which gives a total number of four cases of electrical connections and leads in 36 equivalent circuits cumulatively. So, a total number of 49 equivalent circuits should be investigated.

In each equivalent circuit, the A and B converters can be Bk-, Bk+, Bt-, Bt+, BB- or BB+, as described above, yielding in 36 combinations per equivalent circuit. Hence, a total number of 1764 possible R2P2 non-isolated topologies should be examined to identify which of them are realizable or not.

III. Systematic Investigation of Realizable Non-Isolated R2P2 Topologies

In this section, all the aforementioned analysis is further clarified, taking two different configurations as examples. Applying the same procedure in all 1764 possible combinations, all the realizable non-isolated R2P2 topologies are classified in Table I at the end of this section.

A. Examples of Electrical Connections Cases for I-II and II-III Configurations

To better illustrate the possible electrical connections cases for the R2P2 configurations, I-IIB and IIC-IIIB are taken as examples in this section.

First, for the I-IIB configuration, observing carefully the power flow paths (see Fig. 3) and considering the three rules for realizing the connections of ports and A, B converters, we conclude that $V_{\mathrm{in},A} = V_{\mathrm{in}}$, $V_{o,A} = V_C$, $V_{\mathrm{in},B} = V_{\mathrm{in}}$, and $V_{o,B} = V_o - V_C$, where $V_{\mathrm{in},x}$ and $V_{o,x}$ are the input and output voltages accordingly of the individual converters with $x = A, B$ denoting them, and V_{in}, V_o, and V_C are the input, output, and capacitor voltages (the three ports) of the overall converter, respectively. So, $V_{o,B}$ is composed by the subtraction of $V_{\mathrm{port1}} = V_o$ and $V_{\mathrm{port2}} = V_C$, or alternatively the outputs of A and B converters are in series, forming the overall output voltage. Thus, according to Fig. 4(b), there are two possible cases of electrical connections, namely Cases 1 and 2, as shown in Fig. 6.

Similarly, inspecting the power flow graph for IIC-IIIB configuration, we conclude that $V_{\mathrm{in},A} = V_C$, $V_{o,A} = V_o - V_{\mathrm{in}}$, $V_{\mathrm{in},B} = V_{\mathrm{in}}$, and $V_{o,B} = V_o + V_C$. Therefore, according to Fig. 4, there are four possible cases of electrical connections. More analytically, since $V_{o,A}$ is composed of the subtraction of $V_{\mathrm{port1}} = V_o$ and $V_{\mathrm{port2}} = V_{\mathrm{in}}$, there are two possible subcases of electrical connections for Conv.A, namely Subcase 1A and Subcase 2A. Also, since $V_{o,B}$ is composed by the sum of $V_{\mathrm{port1}} = V_o$ and $V_{\mathrm{port2}} = V_C$, there are other two possible subcases of electrical connections for Conv.B, namely Subcase 1B and Subcase 2B. Thus, combining the aforementioned subcases for the implementation of the total IIC-IIIB configuration, four possible equivalent circuits are formed, namely Subcases 1A, 1B→ Case 1, Subcases 1A, 2B→ Case 2, Subcases 2A, 1B→ Case 3, Subcases 2A, 2B→ Case 4, that are depicted in Fig. 7.

B. Example of Identification of the Realizable Non-Isolated Topologies for I-IIB Configuration

In this section, the R2P2 I-IIB configuration is taken as example in order to identify the combinations of basic converters that lead to implementable non-isolated R2P2 topologies. After creating the equivalent circuits (see Fig. 6), Case 1 [see Fig. 6(a)] is selected as an example for investigation. Hence, a decision tree can be formed, as depicted in Fig. 8, to examine all possible combinations and find the realizable ones for the I-IIB configuration, corresponding to the selected Case 1. Therefore, the realizable topologies produced by Case 1 of I-IIB configuration are Conv. A: Bk- or Bt-, Conv. B: BB- and Conv. A: BB+, Conv. B: Bk+ or Bt+. Similarly, analyzing the Case 2 for I-IIB

TABLE I
NON-ISOLATED R2P2 TOPOLOGIES THAT CAN BE IMPLEMENTED IN REALITY

Configuration	Conv. A	Conv. B	Case	Configuration	Conv. A	Conv. B	Case
I-I	any	any	-	IIA-IIIA	-	-	-
I-IIA	BB+	any	1	IIA-IIIB	BB+	BB+	2
	BB-	any	2		BB-	BB-	3
I-IIB	Bk- / Bt-	BB-	1	IIA-IIIC	Bk-	BB+	2
	BB+	Bk+ / Bt+			Bk+	BB-	3
	Bk+ / Bt+	BB+	2				
	BB-	Bk- / Bt-					
I-IIC	Bt-	Bk+	1	IIB-IIIA	BB-	BB-	2
	Bk+ / Bt+	BB+			BB+	BB+	3
	BB+	Bk- / Bt-		IIB-IIIB	-	-	-
	Bt+	Bk-	2	IIB-IIIC	Bk-	BB-	2
	Bk- / Bt-	BB-			Bk+	BB+	3
	BB-	Bk+ / Bt+		IIC-IIIA	BB-	Bt+	2
I-IIIA	Bk- / Bt-	BB+	1		BB+	Bt-	3
	BB-	Bk+ / Bt+		IIC-IIIB	BB+	Bt+	2
	Bk+ / Bt+	BB-	2		BB-	Bt-	3
	BB+	Bk- / Bt-					
I-IIIB	BB-	any	1	IIC-IIIC	-	-	-
	BB+	any	2				
I-IIIC	Bk-	Bt+	1				
	Bk+ / Bt+	BB-					
	BB-	Bk- / Bt-					
	Bk+	Bt-	2				
	Bk- / Bt-	BB+					
	BB+	Bk+ / Bt+					

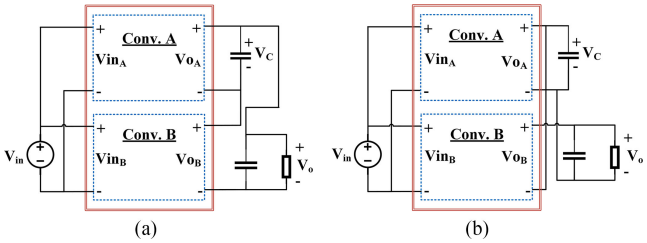

Fig. 6. Two possible cases of electrical connections for investigating the possible topologies in I-IIB configuration. (a) Case 1. (b) Case 2.

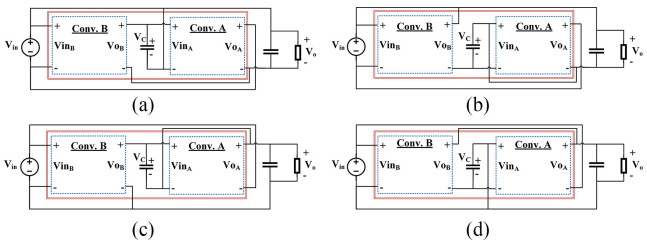

Fig. 7. Four cases of electrical connections for investigating the possible topologies for IIC-IIB configuration. (a) Case 1. (b) Case 2. (c) Case 3. (d) Case 4.

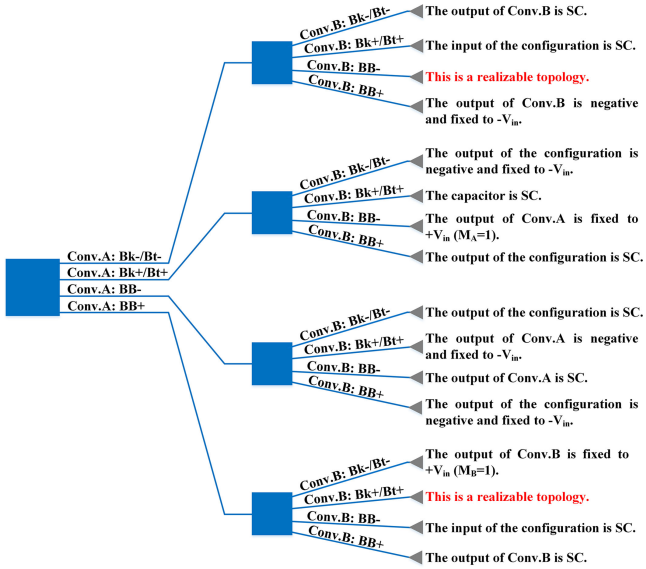

Fig. 8. Decision tree for identifying the implementable non-isolated R2P2 I-IIB topologies, based on Case 1.

configuration, the realizable topologies are Conv. A: Bk+ or Bt+, Conv. B: BB+ and Conv. A: BB-, Conv. B: Bk- or Bt-.

C. Realizable Topologies for All Configurations

Comparing the realizable topologies of the R2P2 I-IIB configuration, it can be concluded that Cases 1 and 2 are complementary. This means that for every realizable topology that belongs to Case 1, there is an equivalent realizable topology belonging to Case 2 and consisted of the same individual A and B converters, which however come from the opposite polarity group than in Case 1. For example, the combination Bk-/BB- is one of the I-IIB realizable topologies belonging to Case 1, where both A and B converters belong to negative polarity group. Then, the equivalent I-IIB Bk+/BB+ topology can be formed, based on Case 2 and the same A, B converters that now belong to the positive polarity group. Furthermore, because of the duality of the electrical connections' cases, the operational characteristics of the topologies belonging to one case of

electrical connections are the same with their complementary counterparts.

After detailed investigation, we conclude that the same applies for all I-II and I-III configurations, i.e., their two cases are complementary. As far as the II-III configurations are concerned, Cases 2 and 3 are also complementary while Cases 1 and 4 do not result in realizable topologies at all. Therefore, the derivation process can be shortened to one case of electrical connections examination per configuration.

Moreover, regarding the configurations IIA-IIIA, IIB-IIIB, and IIC-IIIC, it is noted that while transforming their power flow graphs into equivalent circuits, they were found to be unimplementable for non-isolated topologies, since SC are created, namely:

1) IIA-IIIA: SC of input voltage or capacitor;
2) IIB-IIIB: SC of output voltage or capacitor;
3) IIC-IIIC: SC of Converter B input or Converter A output.

Hence, despite the fact that generally 16 possible R2P2 configurations are reported in the literature, in the case of non-isolated topologies, 13 can produce realizable topologies.

To sum up, all the realizable non-isolated R2P2 topologies (a total resulting number of 108 implementable topologies) are presented in Table I, which can be used as a source for further investigation of various topologies and evaluation of their characteristics and behavior.

IV. Analytical Voltage Gain and Efficiency Calculation of R2P2 Configurations

To complete the analysis for each R2P2 non-isolated configuration, the overall step-up voltage ratio *M* and the efficiency η can be derived from the voltage ratios and efficiencies of the individual converters (M_A, M_B, η_A, η_B, respectively), if we inspect carefully the power flow paths of each configuration, depicted in Fig. 3. The resulting voltage ratio and efficiency are valid for all the equivalent circuits belonging to one configuration. In addition to this, these relations are also valid for both continuous conduction mode (CCM) and discontinuous conduction mode of converters, as proven in authors' previous work [26]. However, since this paper is focused on high-power applications, only CCM has been considered for this work.

Configurations of I-II and I-III types employ only the *k* variable, since one node is present in their power flow graphs, while configurations of II-III type employ both *k* and *m*, since their graphs include two nodes. Calculation of *k* and *m* for all configurations are presented in this paper. Two examples show analytically the procedure of *k, m, η,* and *M* calculation.

A. I-IIB Configuration

Observing Fig. 6, the overall voltage ratio *M* for I-IIB configuration, denoted as $M_{\mathrm{I-IIB}}$, can be calculated as follows:

$$M_{\mathrm{I-IIB}} = \frac{V_o}{V_{\mathrm{in}}} = \frac{V_{o,A}+V_{o,B}}{V_{\mathrm{in}}} = \frac{V_{o,A}}{V_{\mathrm{in}}} + \frac{V_{o,B}}{V_{\mathrm{in}}} = \frac{V_{o,A}}{V_{\mathrm{in},A}} + \frac{V_{o,B}}{V_{\mathrm{in},B}} \Rightarrow M_{\mathrm{I-IIB}} = M_A + M_B. \quad (1)$$

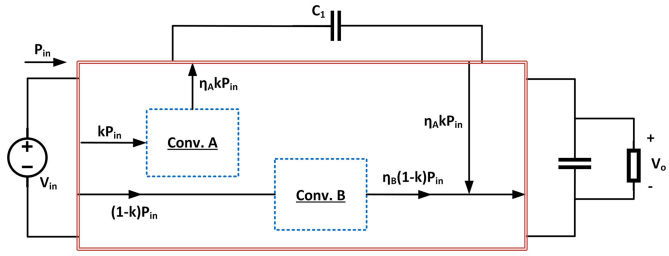

Fig. 9. Power flow paths for the I-IIB configuration.

Considering that the average value of capacitor current is zero under steady-state conditions ($\overline{I_C} = 0$), we can also write

$$I_{o,A} = I_{o,B} = I_o. \quad (2)$$

To calculate the efficiency of I-IIB configuration $\eta_{\mathrm{I-IIB}}$, the power flow paths are depicted in Fig. 9, showing how the input power is split between A and B converters with a portion of *k* and *1 – k* accordingly.

So, based on Fig. 9, the following relations can be extracted:

$$\eta_{\mathrm{I-IIB}} = \frac{P_o}{P_{\mathrm{in}}} = \frac{P_{o,A}+P_{o,B}}{P_{\mathrm{in}}} = \frac{kP_{\mathrm{in}}\eta_A}{P_{\mathrm{in}}} + \frac{(1-k)\,P_{\mathrm{in}}\eta_B}{P_{\mathrm{in}}} \Rightarrow \eta_{\mathrm{I-IIB}} = k\eta_A + (1-k)\,\eta_B. \quad (3)$$

Moreover, based on Figs. 9 and 6

$$\frac{P_{o,A}}{P_{o,B}} = \frac{kP_{\mathrm{in}}\eta_A}{(1-k)\,P_{\mathrm{in}}\eta_B} \Rightarrow \frac{M_A V_{\mathrm{in}} I_o}{M_B V_{\mathrm{in}} I_o} = \frac{k\eta_A}{(1-k)\,\eta_B} \Rightarrow k = \frac{M_A\eta_B}{M_A\eta_B + M_B\eta_A} \quad (4)$$

where $I_{o,x}$, $P_{\mathrm{in},x}$, and $P_{o,x}$ are the output current, input and output power of the individual converters with $x = A, B$ denoting them, while the same symbols without the subscript *x* refer to the overall converter.

Substituting (4) into (3) yields in

$$\eta_{\mathrm{I-IIB}} = \frac{P_o}{P_{\mathrm{in}}} = \eta_A\eta_B\frac{M_A+M_B}{M_A\eta_B + M_B\eta_A}. \quad (5)$$

B. IIC-IIIB Configuration

Similarly, based on the circuit diagram of Case 2 (or Case 3) of Fig. 7, the overall voltage ratio $M_{\mathrm{IIC-IIIB}}$ for IIC-IIIB configuration can be calculated as

$$M_A = \frac{V_{o,A}}{V_{\mathrm{in},A}} = \frac{V_o - V_{\mathrm{in}}}{V_C} \Rightarrow V_C = \frac{V_o - V_{\mathrm{in}}}{M_A} \quad (6)$$

$$M_B = \frac{V_{o,B}}{V_{\mathrm{in},B}} = \frac{V_o + V_C}{V_{\mathrm{in}}} = M_{\mathrm{IIC-IIIB}} + \frac{V_C}{V_{\mathrm{in}}} \overset{(6)}{\Rightarrow} M_{\mathrm{IIC-IIIB}} = \frac{V_o}{V_{\mathrm{in}}} = \frac{M_A M_B + 1}{M_A + 1}. \quad (7)$$

Also, considering that $\overline{I_C} = 0$, the following relations for the currents of A and B as parts of the IIC-IIIB configuration can

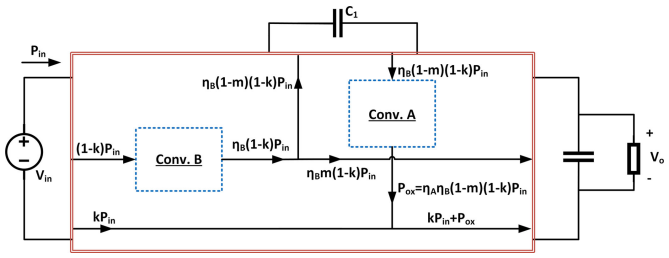

Fig. 10. Power flow paths for the IIC-IIIB configuration.

be written:

$$I_{o,B} = I_{\text{in},A} \tag{8}$$

$$I_o = I_{\text{in},A} + I_{o,A} \overset{(8)}{\Rightarrow} I_o = I_{o,A} + I_{o,B} \tag{9}$$

$$I_{\text{in}} = I_{\text{in},B} + I_{o,A} \tag{10}$$

where $I_{\text{in},x}$ is the input current of individual converters with $x = A$, B denoting them, while the same symbol without the subscript x refers to the overall converter input current.

In Fig. 10, it is shown how the power is split in each branch of the power flow graph for the IIC-IIIB configuration.

Based on Fig. 10, the following relation for the efficiency of IIC-IIIB configuration $\eta_{\text{IIC}-\text{IIIB}}$ can be extracted:

$$\eta_{\text{IIC}-\text{IIIB}} = \frac{\{k + (1-k)\left[\eta_B m + \eta_A \eta_B (1-m)\right]\} P_{\text{in}}}{P_{\text{in}}}$$

$$\Rightarrow \eta_{\text{IIC}-\text{IIIB}} = k + (1-k)\left[\eta_B m + \eta_A \eta_B (1-m)\right]. \tag{11}$$

The portion m can be easily obtained as follows:

$$\frac{P_{o,B}}{P_{\text{in},A}} = \frac{\eta_B (1-k) P_{\text{in}}}{\eta_B (1-k)(1-m) P_{\text{in}}} \overset{(8)}{\Rightarrow} \frac{V_{o,B}}{V_{\text{in},A}} = \frac{1}{1-m}$$

$$\overset{(6),(7)}{\Rightarrow} m = \frac{M_A M_B + 1}{M_B (M_A + 1)}. \tag{12}$$

Moreover, based on Figs. 7 and 10, it can be written

$$P_{o,A} + P_{\text{in},B} = (1-k)\left[\eta_A \eta_B (1-m) + 1\right] P_{\text{in}} \tag{13}$$

$$\overset{(10)}{\Rightarrow} V_{o,A} V_{\text{in}} I_{\text{in}} = V_{o,A} P_{\text{in}} = V_{o,A} P_{\text{in},B} + V_{\text{in}} P_{o,A}$$

$$\overset{(13)}{\Rightarrow} V_{o,A} P_{\text{in}} = (1-k)\left[V_{\text{in}} \eta_A \eta_B (1-m) + V_{o,A}\right] P_{\text{in}}$$

$$\Rightarrow k = \frac{V_{\text{in}}}{V_{o,A}} \eta_A \eta_B (1-k)(1-m)$$

$$\overset{(6),(7)}{\Rightarrow} k = \frac{1}{M_{\text{IIC}-\text{IIIB}} - 1} \eta_A \eta_B (1-k)(1-m). \tag{14}$$

So, substituting (7) and (12) into (14), the quantity k can be extracted

$$k = \frac{\eta_A \eta_B}{\eta_A \eta_B + M_A M_B}. \tag{15}$$

Relations (12) and (15) are substituted into (11), the efficiency of IIC-IIIB is calculated as follows:

$$\eta_{\text{IIC}-\text{IIIB}} = \frac{P_o}{P_{\text{in}}} = \frac{\eta_B (M_A + \eta_A)(M_A M_B + 1)}{(M_A + 1)(M_A M_B + \eta_A \eta_B)}. \tag{16}$$

C. Overall Voltage Ratio and Efficiency for All R2P2 Non-Isolated Configurations

In a similar way, the voltage ratio and efficiency for all R2P2 non-isolated topologies were calculated and tabulated in Table II. Based on this table, one can estimate the voltage gain and efficiency of the overall R2P2 converter, if the voltage gain and efficiency values are available for the individual converters A and B. This will be further illustrated and proven experimentally in Section VI.

V. Selection of a Non-Isolated R2P2 Topology for High Step-Up High-Power Applications

Taking all the aforementioned analysis into account and observing carefully Tables I and II, it can be concluded that configurations I-IIIC, IIA-IIIC, and IIB-IIIC (see Section II-A for nomenclature) result always in voltage step-down topologies. For I-IIIC configuration, this is proven from the relation of M. For IIA-IIIC and IIB-IIIC configurations, Converter A can be only Bk ($M_A < 1$), leading only to step-down topologies.

Furthermore, the configurations I-IIIA and I-IIIB result in voltage gain M lower than M_A or M_B. This is obvious from their relation of M. For IIC-IIIB configuration, Converter B can be only Bt, which means that $M_{\text{B}} > 1$ and so the voltage gain M of this configuration is lower than M_B. Moreover, the configurations IIA-IIIB, IIB-IIIA, and IIC-IIIA result generally in relatively low M and because their possible configurations include BB, the maximum M that can be achieved tends to be $M_{\max} \to M_{BB} + 1$. Therefore, all these six configurations are not suitable for high step-up applications.

Hence, we conclude that I-IIA, I-IIB, and I-IIC have the highest step-up voltage ratio among all. Since high-power applications are the aim of this paper, these three configurations should be also compared in terms of efficiency.

Let us suppose that $\eta_{\text{I}-\text{IIB}} > \eta_{\text{I}-\text{IIC}}$. According to Table II, this means that

$$\eta_A \eta_B \frac{M_A + M_B}{M_A \eta_B + M_B \eta_A} > \eta_A \eta_B \frac{M_A M_B + 1}{M_A M_B + \eta_A \eta_B}$$

$$\Rightarrow M_B \left(M_A^2 - \eta_A\right)(1 - \eta_B) + M_A \left(M_B^2 - \eta_B\right)(1 - \eta_A) > 0. \tag{17}$$

Taking into account that high voltage gain and high efficiency are a prerequisite, M_A and M_B are considered to be greater than 1. Therefore, the above inequality is valid, because $M_A^2 > \eta_A$ and $M_B^2 > \eta_B$. So, the efficiency of I-IIB configuration is higher than the efficiency of I-IIC configuration.

Let us suppose now that $\eta_{\text{I}-\text{IIB}} > \eta_{\text{I}-\text{IIA}}$. According to Table II, this means that

$$\eta_A \eta_B \frac{M_A + M_B}{M_A \eta_B + M_B \eta_A} > \eta_A \eta_B \frac{M_A + 1}{M_A + \eta_A}$$

$$\Rightarrow M_A (1 - \eta_B) + M_B (1 - \eta_A) + \eta_A > \eta_B. \tag{18}$$

This inequality is valid because, generally, η_A and η_B have quite similar values in reality. So, the efficiency of I-IIB configuration is higher than the efficiency of I-IIA configuration.

TABLE II
VOLTAGE RATIO AND EFFICIENCY FOR THE NON-ISOLATED R2P2 CONFIGURATIONS

Configuration	k	m	Voltage ratio *M*	Efficiency η
I-I	1	-	$M_A M_B$	$\eta_A \eta_B$
I-IIA	$\frac{M_A}{M_A+\eta_A}$	-	$M_B(1+M_A)$	$\eta_A \eta_B \frac{M_A+1}{M_A+\eta_A}$
I-IIB	$\frac{M_A \eta_B}{M_A \eta_B + M_B \eta_A}$	-	$M_A + M_B$	$\eta_A \eta_B \frac{M_A+M_B}{M_A \eta_B + M_B \eta_A}$
I-IIC	$\frac{M_A M_B}{M_A M_B + \eta_A \eta_B}$	-	$M_A M_B + 1$	$\eta_A \eta_B \frac{M_A M_B + 1}{M_A M_B + \eta_A \eta_B}$
I-IIIA	$\frac{M_B}{M_A+M_B}$	-	$\frac{M_A M_B}{M_A+M_B}$	$\frac{M_A \eta_B + M_B \eta_A}{M_A+M_B}$
I-IIIB	$\frac{1}{M_A+1}$	-	$\frac{M_A M_B}{M_A+1}$	$\eta_B \frac{M_A+\eta_A}{M_A+1}$
I-IIIC	$\frac{1}{M_A M_B+1}$	-	$\frac{M_A M_B}{M_A M_B+1}$	$\frac{M_A M_B + \eta_A \eta_B}{M_A M_B+1}$
IIA-IIIA	-	-	-	-
IIA-IIIB	$\frac{\eta_B}{\eta_B+M_B}$	$\frac{M_A(1+M_B)}{M_B(1+M_A)}$	$\frac{M_A(1+M_B)}{M_A+1}$	$\eta_B \frac{(M_A+\eta_A)(M_B+1)}{(M_A+1)(M_B+\eta_B)}$
IIA-IIIC	$\frac{\eta_B}{\eta_B+M_B}$	$\frac{M_A(1+M_B)}{M_A M_B+1}$	$\frac{M_A(1+M_B)}{M_A M_B+1}$	$\frac{(M_A M_B + \eta_A \eta_B)(M_B+1)}{(M_A M_B+1)(M_B+\eta_B)}$
IIB-IIIA	$\frac{M_A}{\eta_A+M_A}$	$\frac{M_B-M_A}{M_B+1}$	$\frac{M_B(1+M_A)}{M_B+1}$	$\frac{\eta_A(M_A+1)(M_B+\eta_B)}{(M_A+\eta_A)(M_B+1)}$
IIB-IIIB	-	-	-	-
IIB-IIIC	$\frac{M_A \eta_B}{M_A \eta_B + M_B \eta_A}$	$\frac{M_A+M_B}{M_B+1}$	$\frac{M_A+M_B}{M_B+1}$	$\frac{\eta_A(M_A+M_B)(M_B+\eta_B)}{(M_B+1)(M_A \eta_B + M_B \eta_A)}$
IIC-IIIA	$\frac{M_A}{\eta_A+M_A}$	$\frac{M_A+1}{M_A+M_B}$	$\frac{M_B(1+M_A)}{M_A+M_B}$	$\frac{(M_A+1)(M_A \eta_B + M_B \eta_A)}{(M_A+\eta_A)(M_A+M_B)}$
IIC-IIIB	$\frac{\eta_A \eta_B}{M_A M_B + \eta_A \eta_B}$	$\frac{M_A M_B+1}{M_B(1+M_A)}$	$\frac{M_A M_B+1}{M_A+1}$	$\frac{\eta_B(M_A+\eta_A)(M_A M_B+1)}{(M_A+1)(M_A M_B + \eta_A \eta_B)}$
IIC-IIIC	-	-	-	-

Therefore, the highest efficiency is within I-IIB. Hence, I-IIB is chosen in this paper for further investigation, since it exhibits a good tradeoff between high step-up ratio and high efficiency and so it is suitable for high-power high step-up ratio applications that this work aims for.

The four implementable non-isolated topologies of I-IIB configuration, namely Bk-/ BB-, Bt-/ BB-, BB+/ Bk+, and BB+/ Bt+ (see Table I), are depicted in Fig. 11. The topologies (a), (c) and (b), (d) are equivalent as far as the functionality is concerned. However, the topologies (a), (c) have lower *M* compared to (b), (d), since they include Bk converter and *M* is the sum of M_A, M_B. Therefore, we choose the topologies (b), (d). In fact, since capacitor C_1 does not affect the steady-state characteristics of the converter, the two topologies (Bt-/ BB- and BB+/ Bt+) are equivalent. However, in Bt-/BB- topology, the voltage stress in this capacitor is higher $[V_C = (V_o + V_{\text{in}})/2]$ than in BB+/Bt+ $[V_C = (V_o - V_{\text{in}})/2]$. Therefore, the topology I-IIB BB+/Bt+, which is redesigned in Fig. 12 for simplicity reasons, is chosen here as the most promising candidate for high-power high step-up applications.

When the switches S_1, S_2 are turned ON, the inductors L_1, L_2 are charged in parallel from the dc source. The energy demand from the load R_o is covered by the output capacitor C_o. When the switches are turned OFF, the two inductors are connected in series through the diodes D_1, D_2, releasing their energy to the load and the output capacitor.

VI. EXPERIMENTAL RESULTS

A. Specifications and Design Guidelines of the Experimental Prototype

To validate the presented theoretical analysis and above-calculated relationships, as well as the functionality of the chosen converter in high power, experimental results are conducted in a prototype made in the laboratory. In order to specify the design characteristics of the experimental prototype for a high step-up high-power application, we consider a WHRS with TEGs for a ship with a dc bus of 625 V [29]. The R2P2 I-IIB BB+/Bt+ converter is employed for the interconnection of TEGs to the dc bus. Therefore, it is desired to evaluate its

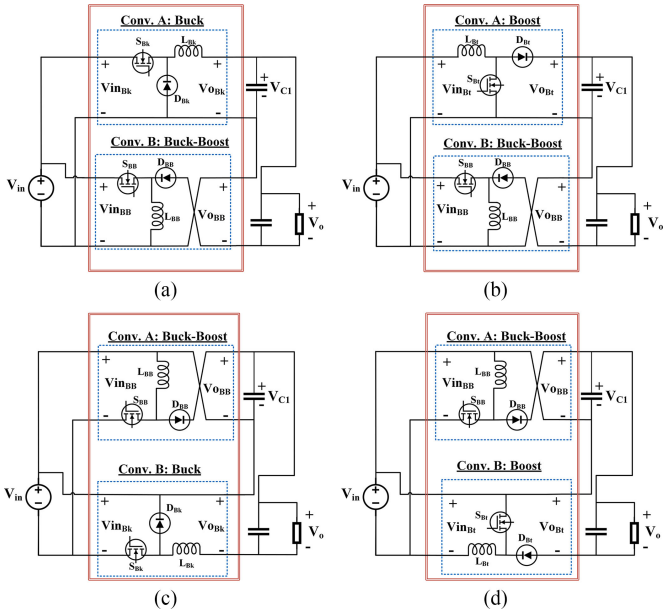

Fig. 11. Four realizable non-isolated topologies for I-IIB configuration of R2P2 family.

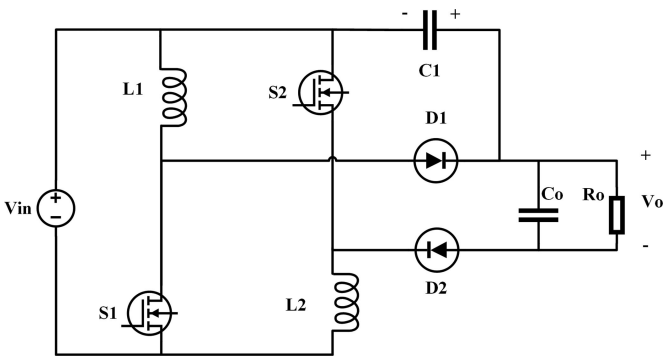

Fig. 12. Non-Isolated R2P2 I-IIB BB+/Bt+ converter.

efficiency under various step-up voltage ratios, while keeping the output voltage constant at $V_o = 625$ V.

In addition to this, experimental results are conducted on the individual converters BB and Bt as parts of the I-IIB BB+/Bt+ topology in order to investigate the percentage of the total power that each converter is handling and so to validate the theoretical analysis presented in Sections III and IV.

Hence, a 2-kW prototype of the R2P2 I-IIB BB+/Bt+ dc/dc converter, shown in Fig. 13, was designed and built with the intention to operate in different input voltage levels. Special attention was given to the design of the printed circuit, so as to achieve low inductance layout, enabling fast switching with minimal ringing. The converter is controlled with the microcontroller TMS320F28335. The power analyzer LMG500 was employed in the setup for accurate measurements.

For our application, the two inductors of the converter are chosen to be of the same value for symmetrical functionality. Also, to have a simple driver circuit, we consider that the switches are fired simultaneously, with the same duty cycle d. Considering that the two individual converters are operating in CCM and so

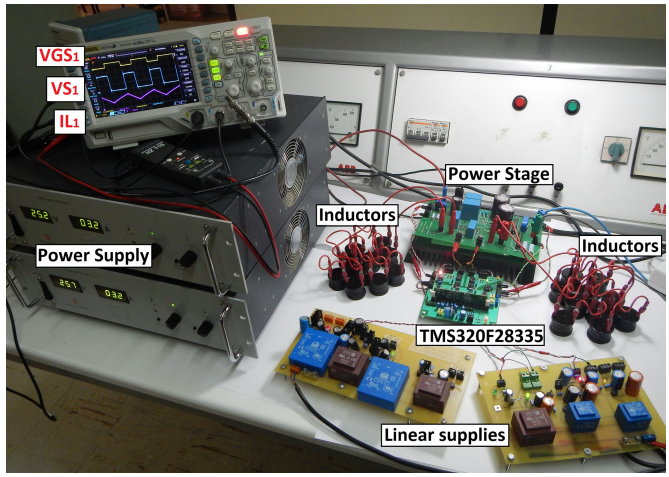

Fig. 13. 2-kW prototype of the I-IIB BB+/Bt+ converter.

TABLE III
CALCULATION OF INDUCTORS VALUE FOR CCM OPERATION OF THE CONVERTER UNDER VARIOUS VOLTAGE RATIOS

M	V_{in} (V)	d	L_{min} (uH)	L_{chosen} (uH)
5	125	0.667	868.1	900
7	89.28	0.75	523.2	600
9	69.44	0.8	347.2	400
11	56.82	0.833	246.6	300
13	48.08	0.857	183.9	200

the overall I-IIB converter does, and based on (3), as well as the ideal voltage ratios of BB and Bt, we can write

$$M_{\mathrm{BB}/Bt}^{\mathrm{I-IIB}} = \frac{V_o}{V_{\mathrm{in}}} = M_{\mathrm{BB}} + M_{Bt} = \frac{d}{1-d} + \frac{1}{1-d} = \frac{1+d}{1-d}$$

$$\Rightarrow d = \frac{M_{\mathrm{BB}/Bt}^{\mathrm{I-IIB}} - 1}{M_{\mathrm{BB}/Bt}^{\mathrm{I-IIB}} + 1}. \tag{19}$$

For the experimental results, we set as common criterion that the converter should operate at CCM from 10% of its nominal power P_N and above, for each overall voltage ratio M under constant switching frequency $f_s = 50$ kHz. To assure the operation of converter in CCM, the minimum needed inductors value $L_{1,\min} = L_{2,\min} = L_{\min}$ has been calculated, using the following relation [30]:

$$L_{1,\min} = L_{2,\min} = L_{\min} \geq \frac{V_o^2 d(1-d)^2}{2P_{o|\min} f_s}. \tag{20}$$

Therefore, considering constant the values of $P_{o|\min} = 10\% P_N = 10\% \cdot 2\,\mathrm{kW} = 200\,\mathrm{W}$ and $V_o = 625\,\mathrm{V}$ while M changes, V_{in} and so d must change accordingly. This dictates different inductor value for each M, calculated in Table III, using (19) and (20).

L_{chosen} are the inductors values used in the experimental prototype. Since many different setups should be evaluated, commercial inductor units of 100 μH (1140–101K-RC) are combined in parallel and/or series to achieve the L_{chosen} values and to meet the current ratings.

TABLE IV
CONVERTER COMPONENTS FOR EFFICIENCY EVALUATION

Component	Type
S_1, S_2	SCH2080KEC, 1200 V, 40 A, 80 mΩ
D_1, D_2	STPSC20065D, 650 V, 20 A
L_1, L_2	1140-101K-RC, 100 uH, I_{rms}=10.5 A, I_{sat}=20.6 A
C_1	50 uF
C_o	280 uF

TABLE V
STEP-UP RATIOS AND VOLTAGE OUTPUT FOR INDIVIDUAL CONVERTERS

M	d	M_{BB}	M_{Bt}	$V_{in} = V_{in,BB} = V_{in,Bt}$ (V)	$V_{o,BB}$ (V)	$V_{o,Bt}$ (V)
5	0.667	2	3	125	250	375
7	0.75	3	4	89.28	267.84	357.12
9	0.8	4	5	69.44	277.76	347.2
11	0.833	5	6	56.82	284.1	340.92
13	0.857	6	7	48.08	288.48	336.56

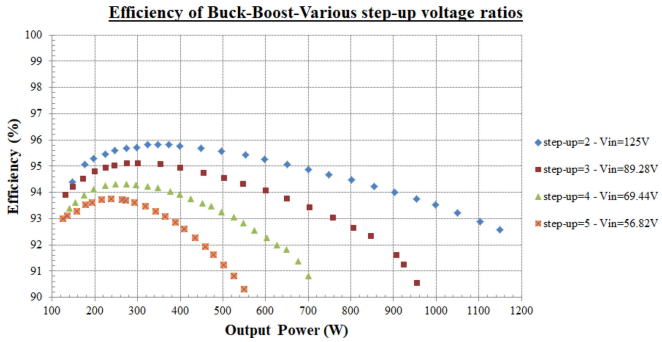

Fig. 14. Efficiency of BB converter under various step-up voltage ratios and a high-power range.

The components chosen for the prototype are shown in Table IV. The employed semiconductor devices are of SiC, so as to achieve minimum switching losses and small heatsink. High voltage-breakdown transistors were chosen for this prototype to assure the safe operation of the converter, even in possible over-voltages/spikes. This means that the prototype was built mainly for demonstrating the functionality of an R2P2 converter and it is not necessarily an optimal design.

Calculating the needed duty cycle for each desired step-up voltage ratio of the overall converter (see Table III), it is possible to determine the step-up voltage ratios of the individual converters as well as their output voltage, since $V_{\rm in} = V_{{\rm in},A} = V_{{\rm in},B}$. These calculations are shown in Table V for various step-up voltage ratios of the R2P2 I-IIB BB+/Bt+ converter.

B. Experimental Evaluation of I-IIB BB+/Bt+ Converter Efficiency

Based on Table V, experimental results were conducted for BB and Bt converters separately to evaluate their efficiency for various step-up voltage ratios, as shown in Figs. 14 and 15, respectively.

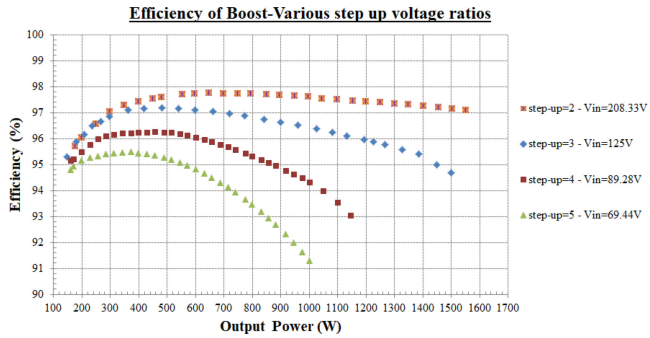

Fig. 15. Efficiency of Bt converter under various step-up voltage ratios and a high power range.

TABLE VI
ESTIMATION OF I-IIB BB+/BT+ EFFICIENCY FROM INDIVIDUAL CONVERTERS CHARACTERISTICS

M	V_{in} (V)	M_{BB}	M_{Bt}	$P_{o,BB}$ (W)	$P_{o,Bt}$ (W)	η_{BB} (%)	η_{Bt} (%)	k_{calc} (%)	η_{I-IIB}^{calc} (%)
5	125	2	3	400	600	95.8	97.1	40.3	96.5
7	89.3	3	4	428.6	571.4	94.9	96.1	43.2	95.6
9	69.4	4	5	444.5	555.6	93.6	95	44.8	94.4

Hence, for a given step-up voltage ratio and output power of the overall R2P2 converter and considering that $I_o = I_{o,A} = I_{o,B}$ (4), it is possible to specify the output power of each one of the incorporated converters on the R2P2 I-IIB BB+/Bt+ topology. This is further clarified in Table VI, where analytical calculations are shown as example, for three different step-up voltage ratios and for 1-kW total output power, namely output current of 1.6 A. Knowing the efficiency and the voltage ratios of the individual converters for the calculated power (see Figs. 14 and 15), we can apply (4) and (5) to calculate k and the efficiency of I-IIB BB+/Bt+ topology, shown as $k_{\rm calc}$ and $\eta_{\rm I-IIB}^{\rm calc}$ in Table VI, respectively.

It is worth noticing that the higher the overall step-up voltage ratio, the bigger the k value becomes. This means that higher percentage of the total input power is processed by the BB which generally has lower efficiency than Bt (see Figs. 14 and 15). So, it is expected that the efficiency of the R2P2 I-IIB BB+/Bt+ converter drops when step-up voltage ratio is increased.

Applying the same calculations for the whole range of output power of I-IIB converter, it is possible to theoretically calculate its efficiency from the individual converters' characteristics. Experimental results for the efficiency of the overall I-IIB BB+/Bt+ converter are presented in Fig. 16 along with their calculated values for the three aforementioned step-up ratios for comparison.

It is obvious that the experimental and estimated values of the efficiency of R2P2 I-IIB BB+/Bt+ converter are well matched, which proves the validity of the aforementioned theoretical analysis and calculations. Furthermore, it is verified that the R2P2 I-IIB BB+/Bt+ converter can operate with high efficiency and high voltage gain, in a high-power range, making it suitable for high-power high step-up applications.

The gate–source and drain–source voltage waveforms of transistor S_1 and current waveform of inductor L_1 are shown in

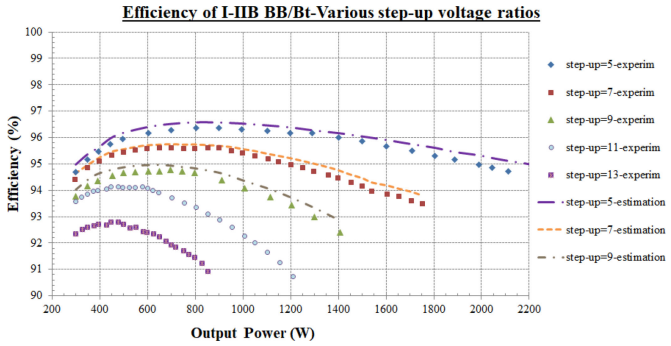

Fig. 16. Efficiency of the R2P2 I-IIB BB+/Bt+ converter under various step-up voltage ratios and a high-power range.

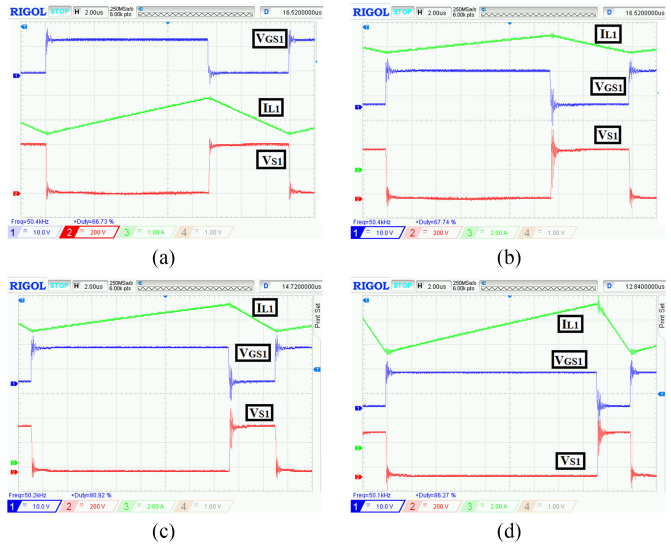

Fig. 17. Transistors voltage and inductors current waveforms of the R2P2 I-IIB BB+/Bt+ converter for (a) $M = 5$ and $P_o = 600$ W, (b) $M = 5$ and $P_o = 2000$ W, (c) $M = 9$ and $P_o = 1400$ W, and (d) $M = 13$ and $P_o = 800$ W.

Fig. 17 for different step-up voltage ratios (5, 9, and 13) and various output power levels. It is proven that the converter operates well, due to the improved layout design, even in such high step-up ratio, high power and high duty cycle [$d \cong 0.863$ in Fig. 17(d)]. Also, it is confirmed that the converter operates in CCM region for all cases.

VII. Conclusion

In this paper, a systematic investigation for non-isolated topologies of the R2P2 family of converters was conducted to identify all the realizable non-isolated topologies and to find a suitable one for high voltage gain high-power applications. Moreover, relations for the voltage ratio and efficiency for every configuration were also extracted. Analytical examples clarified each step of this study. The analysis showed that 13 out of 16 R2P2 configurations can produce implementable non-isolated topologies. Also, three out of them result in voltage step-down topologies, while other six configurations produce step-up topologies but with low voltage gain. Among the remaining R2P2 configurations, the topology I-IIB BB+/Bt+ was selected, because it exhibits a good combination of high step-up ratio and high efficiency for high-power applications. Experiments conducted in a 2-kW prototype proved its high efficiency for various step-up ratios and in a high-power range, and so its suitability for high-power applications, such as WHRSs. What is more, the theoretical analysis and calculation of the efficiency of the overall converter was validated through experimental results conducted separately on its individual converters.

References

[1] R. Sekar, D. S. Suresh, and H. Naganagouda, "A review on power electronic converters suitable for renewable energy sources," in *Proc. Int. Conf. Elect. Electron. Commun. Comput. Optim. Techn.*, 2017, pp. 501–506.

[2] A. Marzouki, M. Hamouda, and F. Fnaiech, "A review of PWM voltage source converters based industrial applications," in *Proc. Int. Conf. Elect. Syst. Aircraft Railway Ship Propulsion Road Veh.*, 2015, pp. 1–6.

[3] Y. Zhang, Y. Gao, L. Zhou, and M. Sumner, "A switched-capacitor bidirectional DC-DC converter with wide voltage gain range for electric vehicles with hybrid energy sources," *IEEE Trans. Power Electron.*, vol. 33, no. 11, pp. 9459–9469, Nov. 2018.

[4] B. K. Bose, "Power electronics, smart grid and renewable energy systems," *Proc. IEEE*, vol. 105, no. 11, pp. 2011–2018, Sep. 2017.

[5] F. L. Luo and H. Ye, *Advanced DC/DC Converters*. Boca Raton, FL, USA: CRC Press, 2004.

[6] M. Forouzesh, Y. P. Siwakoti, S. A. Gorji, F. Blaabjerg, and B. Lehman, "Step-Up DC–DC converters: A comprehensive review of voltage boosting techniques, topologies, and applications," *IEEE Trans. Power Electron.*, vol. 32, no. 12, pp. 9143–9178, Dec. 2017.

[7] C.-M. Young, M.-H. Chen, T.-A. Chang, C.-C. Ko, and K.-K. Jen, "Cascade Cockcroft–Walton voltage multiplier applied to transformerless high step-up DC–DC converter," *IEEE Trans. Ind. Electron.*, vol. 60, no. 2, pp. 523–537, Feb. 2013.

[8] A. Shahin, J.-P. Martin, B. Nahid-Mobarakeh, and S. Pierfederici, "Optimal efficiency operation of non-isolated DC/DC converter for high voltage ratio applications," in *Proc. 39th Annu. Conf. IEEE Ind. Electron. Soc.*, 2013, pp. 1106–1111.

[9] F. L. Tofoli, D. de Castro Pereira, W. Josias de Paula, and D. de Sousa Oliveira Júnior, "Survey on non-isolated high-voltage step-up DC-DC topologies based on the boost converter," *IET Power Electron.*, vol. 8, no. 10, pp. 2044–2057, Sep. 2015.

[10] H. Matsuo and K. Harada, "The cascade connection of switching regulators," *IEEE Trans. Ind. Appl.*, vol. IA-12, no. 2, pp. 192–198, Mar. 1976.

[11] J. A. Morales-Saldaña, E. E. C. Gutierrez, and J. Leyva-Ramos, "Modeling of switch-mode DC-DC cascade converters," *IEEE Trans. Aerosp. Electron. Syst.*, vol. 38, no. 1, pp. 295–299, Jan. 2002.

[12] C. K. Tse and M. H. L. Chow, "A theoretical examination of the circuit requirements of power factor correction," in *Proc. 29th Annu. IEEE Power Electron. Spec. Conf.*, vol. 2, 1998, pp. 1415–1421.

[13] C. K. Tse and M. H. L. Chow, "Theoretical study of switching power converters with power factor correction and output regulation," *IEEE Trans. Circuits Syst. I, Fundam. Theory Appl.*, vol. 47, no. 7, pp. 1047–1055, Jul. 2000.

[14] C. K. Tse and M. H. L. Chow, "Classification and derivation of switching power converters with power factor correction and output regulation," in *Proc. 3rd Int. Power Electron. Motion Control Conf.*, vol. 2, 2000, pp. 574–577.

[15] C. K. Tse, M. H. L. Chow, and M. K. H. Cheung, "A family of PFC voltage regulator configurations with reduced redundant power processing," *IEEE Trans. Power Electron.*, vol. 16, no. 6, pp. 794–802, Nov. 2001.

[16] C. K. Tse, M. H. L. Chow, and M. K. H. Cheung, "Reduced redundant power processing PFC voltage regulators: Circuit synthesis and control," in *Proc. 31st Annu. IEEE Power Electron. Spec. Conf.*, vol. 2, 2000, pp. 825–830.

[17] M. H. L. Chow and C. K. Tse, "An efficient PFC voltage regulator with reduced redundant power processing," in *Proc. 30th Annu. IEEE Power Electron. Spec. Conf.*, vol. 1, 1999, pp. 87–92.

[18] R. Velasco-Reyes, R. Loera-Palomo, M. A. Rivero-Corona, F. S. Sellschopp-Sanchez, and J. A. Morales-Saldaña, "Three-Phase converter based on reduced redundant power processing concept," in *Proc. IEEE Int. Autumn Meeting Power Electron. Comput.*, 2017, pp. 1–6.

[19] M. K. H. Cheung, M. H. L. Chow, and C. K. Tse, "A 1-kW isolated noncascaded boost buck-boost AC/DC PFC power supply based on reduced redundant power processing principle," in *Proc. 24th Annu. Int. Telecommun. Energy Conf.*, 2002, pp. 619–626.
[20] M. K. H. Cheung, M. H. L. Chow, and C. K. Tse, "Practical design and evaluation of a 1 kW PFC power supply based on reduced redundant power processing principle," *IEEE Trans. Ind. Electron.*, vol. 55, no. 2, pp. 665–673, Feb. 2008.
[21] C. Gobbato, G. W. Denardin, and J. de Pelegrini Lopes, "Comparison between stages connections of DC converters for street lighting system based on LED," in *Proc. IEEE 8th Int. Symp. Power Electron. Distrib. Gener. Syst.*, 2017, pp. 1–6.
[22] R. Loera-Palomo and J. A. Morales-Saldana, "Family of quadratic step-up DC-DC converters based on noncascading structures," *IET Power Electron*., vol. 8, no. 5, pp. 793–801, May 2015.
[23] J. A. Morales-Saldaña, R. Loera-Palomo, E. Palacios-Hernández, and J. L. González-Martínez, "Modeling and control of a DC–DC quadratic boost converter with R2P2," *IET Power Electron*., vol. 7, no. 1, pp. 11–22, Jan. 2014.
[24] E. A. Moreno-Basaldua, J. A. Morales-Saldana, and R. Loera-Palomo, "Design methodology for quadratic step-up DC-DC converters based on non-cascading structures," in *Proc. 13th Int. Conf. Power Electron.*, 2016, pp. 210–215.
[25] C. P. Delgado-Antillon, J. A. Morales-Saldana, R. Pena-Gallardo, E. Moreno-Basaldua, and R. Loera-Palomo, "Optimized design of a quadratic boost converter based on the R2P2 principle," in *Proc. IEEE Int. Autumn Meeting Power Electron. Comput.*, 2016, pp. 1–6.
[26] C. G. Zogogianni, and E. C. Tatakis, "Behavioral analysis of a DC/DC single-switch high step-up R2P2 buck-boost/boost converter," in *Proc. 20th Eur. Conf. Power Electron. Appl.*, 2018, pp. 1–10.
[27] M. N. Pefkianaki, C. G. Zogogianni, and E. C. Tatakis, "Investigation of the operational behavior of a DC/DC high step up R2P2 converter," in *Proc. Panhellenic Conf. Electron. Telecommun.*, 2017, pp. 1–4.
[28] P. Yang, C. K. Tse, J. Xu, and G. Zhou, "Synthesis and analysis of double-input single-output DC/DC converters," *IEEE Trans. Ind. Electron.*, vol. 62, no. 10, pp. 6284–6295, Oct. 2015.
[29] N. A. Zarkadis, C. G. Zogogianni, and E. C. Tatakis, "Investigation of the behavior of a high step-up DC/DC converter used in a waste heat recovery system, for marine applications," in *Proc. 18th Eur. Conf. Power Electron. Appl.*, 2016, pp. 1–10.
[30] C. G. Zogogianni, N. A. Zarkadis, and E. C. Tatakis, "Energy savings in marine applications using thermoelectric modules and high step-up DC/DC converter," in *Proc. 8th IET Int. Conf. Power Electron. Mach. Drives*, 2016, pp. 1–5.

Charoula G. Zogogianni is from Pyrgos Ileias, Greece. She received the Diploma degree in electrical engineering from the University of Patras, Rion-Patras, Greece, in 2013, where she is currently working toward the doctorate degree.

Her research interests include energy savings in transportation, renewable energy systems, dc/dc converters analysis and investigation.

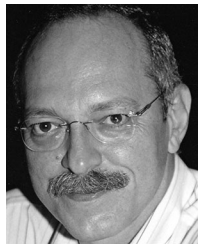

Emmanuel C. Tatakis received the Diploma degree in electrical engineering from the University of Patras, Rion-Patras, Greece, in 1981, and the Ph.D. degree in applied sciences from the University of Brussels, Brussels, Belgium, in 1989.

He is currently a Professor with the Department of Electrical and Computer Engineering, University of Patras. His teaching activities include power electronics and electrical machines. His research interests include switch-mode power supplies, dc/dc converters analysis, electric drive systems and electric vehicles, renewable energy systems, energy saving, power quality, power factor correction, educational methods in electrical machines and power electronics.

Dr. Tatakis is a Member of the European Power Electronics Association and the Technical Chamber of Greece.

Marko S. Vekic received the Ph.D. degree in electrical engineering from the Faculty of Technical Sciences, University of Novi Sad, Novi Sad, Serbia, in 2014.

He has been an Assistant Professor with the Department of Power, Electronic and Telecommunication Engineering, University of Novi Sad, since 2014. His research interests include grid-connected converters, microgrids and power quality. He also participated in designing several advanced solutions for power electronics research and development such as hardware in the loop (HIL) emulators and launch ramp (LARA) systems.